Research Article | Vol. 26, No. 20 | 1 Oct 2018 | OPTICS EXPRESS 25892
Optics EXPRESS

Line of sight calibration for the laser ranging interferometer on-board the GRACE Follow-On mission: on-ground experimental validation

ALEXANDER KOCH,[1,*] JOSEP SANJUAN,[2] MARTIN GOHLKE,[2] CHRISTOPH MAHRDT,[1] NILS BRAUSE,[1] CLAUS BRAXMAIER,[2,3] AND GERHARD HEINZEL[1]

[1] *Max Planck Institute for Gravitational Physics (Albert Einstein Institute) and Institut f. Gravitationsphysik der Leibniz Universität Hannover, Callinstr. 38, 30167 Hannover, Germany*
[2] *German Aerospace Center (DLR), Robert Hooke Str. 7, 28359 Bremen, Germany*
[3] *Center of Applied Space Technology and Microgravity (ZARM), University of Bremen, Am Fallturm 1, 28359 Bremen, Germany*
[*] *alexander.koch@aei.mpg.de*

Abstract: The laser ranging interferometer (LRI) on board of the GRACE follow-on spacecraft, launched in May 2018, is the first laser interferometer to perform an inter-satellite range measurement. It is designed for ranging noise levels of 80 nm $Hz^{-1/2}$ for frequencies above 20 mHz, i.e., about a ten-fold improvement with respect to the GRACE follow-on main microwave ranging instrument. One of the most critical steps during the commissioning phase of the instrument is the so-called initial line of sight calibration procedure (or initial acquisition). This process is required to quantify large uncertainties with respect to laser beam pointing angles and laser frequency, which must be known to establish the interferometer link. It is a nine hour scan of five degrees of freedom, which all need to match simultaneously at least once. Here we report on laboratory tests to further validate the calibration procedure using a mock-up LRI and a set-up, the so-called laser link simulator, that creates conditions similar to those with ~220 km distance between the SC. The experiments presented here made use of LRI-like hardware and software and were carried out recreating critical conditions such as received laser powers on the pico-Watt level and their dependence on the SC misalignments, flat-top beams as receiving beams and Doppler frequency shifts. Several configurations were tested, including a full line of sight calibration with angular scans in both mock-up SC and frequency scan in one of the lasers. Results are well in agreement with the expectations and confirm, well before the LRI commissioning phase, the robustness of the procedure under realistic conditions, which had not yet been fully tested experimentally.

OCIS codes: (120.3180) Interferometry; (120.6085) Space instrumentation; (280.4788) Optical sensing and sensors.

References and links

1. B. D. Tapley, S. Bettadpur, M. Watkins, and C. Reigber, "The gravity recovery and climate experiment: mission overview and early results," Geophys. Res. Lett. **31**, L09607 (2004.)
2. B. S. Sheard, G. Heinzel, K. Danzmann, D. A. Shaddock, W. M. Klipstein, and W. M. Folkner, "Intersatellite laser ranging instrument for the GRACE Follow-On mission," J. Geod. **86**, 1083–1095 (2012.)
3. C. Mahrdt, "Laser link acquisition for the GRACE Follow-On laser ranging interferometer," PhD Thesis, Leibniz Universität Hannover (2014.)
4. D. M. R. Wuchenich, C. Mahrdt, B. S. Sheard, S. Francis, R. Spero, J. Miller, C. Mow-Lowry, R. Ward, W. M. Klipstein, G. Heinzel, K. Danzmann, D. McClelland, and D. A. Shaddock, "Laser link acquisition demonstration for the GRACE Follow-On mission," Opt. Express **22**, 11351–11366 (2014.)
5. D. M. R. Wuchenich, "Inter-satellite laser interferometry," PhD Thesis, Australian National University (2014.)
6. J. Sanjuan, M. Gohlke, S. Rasch, K. Abich, A. Görth, G. Heinzel, and C. Braxmaier,"Interspacecraft link simulator for the laser ranging interferometer onboard GRACE Follow-On," Appl. Opt. **54**, 6682–6689 (2015.)
7. M. Armano, M. Benedetti, J. Bogenstahl, D. Bortoluzzi, P. Bosetti, N. Brandt, A. Cavalleri, G. Ciani, I. Cristofolini, A. M. Cruise, K. Danzmann, I. Diepholz, G. Dixon, R. Dolesi, J. Fauste, L. Ferraioli, D. Fertin, W. Fichter, M. Freschi,

#335651 https://dx.doi.org/10.1364/OE.26.025892
Journal © 2018 Received 20 Jun 2018; revised 13 Aug 2018; accepted 14 Aug 2018; published 19 Sep 2018

Optics EXPRESS

A. García, C. García, A. Grynagier, F. Guzmán, E. Fitzsimons, G. Heinzel, M. Hewitson, D. Hollington, J. Hough, M. Hueller, D. Hoyland, O. Jennrich, B. Johlander, C. Killow, A. Lobo, D. Mance, I. Mateos, P. W. McNamara, A. Monsky, D. Nicolini, D. Nicolodi, M. Nofrarias, M. Perreur-Lloyd, E. Plagnol, G. D. Racca, J. Ramos-Castro, D. Robertson, J. Sanjuan, M. O. Schulte, D. N. A. Shaul, M. Smit, L. Stagnaro, F. Steier, T. J. Sumner, N. Tateo, D. Tombolato, G. Vischer, S. Vitale, G. Wanner, H. Ward, S. Waschke, V. Wand, P. Wass, W. J. Weber, T. Ziegler, and P. Zweifel, "LISA Pathfinder: the experiment and the route to LISA," Class. Quantum Grav. **26**, 094001 (2009.)

8. B. Bachman, G. de Vine, J. Dickson, S. Dubovitsky, J. Liu, W. Klipstein, K. McKenzie, R. Spero, A. Sutton, B. Ware, and C. Woodruff,"Flight phasemeter on the laser ranging interferometer on the GRACE Follow-On mission," IOP Conf. Series: Journal of Physics: Conf. Series **840**, 012011 (2017.)
9. R. Thompson, W. M. Folkner, G. deVine, W. M. Klipstein, K. McKenzie, R. Spero, N. Yu, M. Stephens, J. Leitch, and R. Pierce, "A flight-like optical reference cavity for GRACE Follow-on laser frequency stabilization," *2011 Joint Conference of the IEEE International Frequency Control and the European Frequency and Time Forum (FCS) Proceedings* (IEEE, 2011.)
10. D. Schütze, D. Farrant, D. A. Shaddock, B. S. Sheard, G. Heinzel, and K. Danzmann, "Measuring coalignment of retroreflectors with large lateral incoming-outgoing beam offset," Rev. Sci. Instrum. **85**, 035103 (2014.)
11. D. Schütze, "Intersatellite laser interferometry: test environments for GRACE Follow-On," PhD Thesis, Leibniz Universität Hannover (2015.)
12. D. Z. Anderson,"Alignment of resonant optical cavities," Appl. Opt. **23**, 2944–2949 (1984.)
13. D. Schütze, G. Stede, V. Müller, O. Gerberding, T. Bandikova, B. S. Sheard, G. Heinzel, and K. Danzmann, "Laser beam steering for GRACE Follow-On intersatellite interferometry," Opt. Express **22**, 24117–24132 (2014.)
14. T. T. Hyde, P. G. Maghami, and S. M. Merkowitz, "Pointing acquisition and performance for the laser interferometry space antenna mission," Class. Quantum Grav. **21**, 635–640 (2014.)
15. L. Ziren, Q. Wang, C. Mahrdt, A. Görth, and G. Heinzel, "Possible alternative acquisition scheme for the gravity recovery and climate experiment follow-on-type mission," Appl. Opt. **56**, 1495–1500 (2017.)
16. P. G. Maghami, T. T. Hyde, and J. Kim, "An acquisition control for the laser interferometer space antenna," Class. Quantum Grav. **22**, 421–428 (2005.)
17. N. C. Brause, "Auxiliary function development for the LISA metrology system," PhD Thesis, Leibniz Universität Hannover (2018.)
18. G. Fernández Barranco, O. Gerberding, T. Schwarze, B. S. Sheard, C. Dahl, B. Zender, and G. Heinzel, "Phase stability of photoreceivers in intersatellite laser interferometers," Opt. Express **25**, 7999–8010 (2017.)

1. Introduction

The Gravity Recovery and Climate Experiment (GRACE) [1] was a successful satellite mission launched in 2002. Due to ageing of the spacecraft (SC) batteries, the mission finally came to an end in late 2017 after more than tripling its mission design time. Since its launch the two SC have been monitoring the Earth's gravity field changes in order to gain understanding in a variety of topics such as the mass loss of polar ice sheets, sea level rise due to water mass influx, changes in hydrological cycles, underground water storage, etc. GRACE used a microwave dual-one way ranging to track the intersatellite distance with micrometer resolution. From this quantity temporal and spatial variations of the Earth's gravity field, caused mostly by water movement, were obtained on a monthly basis. The underlying measurement idea is that mass concentrations on the Earth, and their alteration, exert different forces on the two SC, thus affecting their separation.

On May 22nd, 2018 the mission GRACE Follow-On was launched. It was decided to launch the successor mission to GRACE with the smallest possible time gap to ensure data continuity. This could only be achieved by keeping the measurement principle the same as for GRACE and by relying on proven instruments: two SC track their separation on a polar low-Earth orbit with a mean separation of about 220 km using a microwave ranging instrument as the main science instrument. However, a laser-based ranging instrument, the so-called laser ranging interferometer (LRI), was added to the architecture as a technology demonstrator, designed to be able to determine the intersatellite distance with noise levels around 80 nm $\mathrm{Hz}^{-1/2}$ at frequencies above 20 mHz [2], i.e. more than a 10-fold improvement with respect to the microwave ranging instrument.

The most critical step in the commissioning phase of the LRI is the so-called initial line of sight (LOS) calibration. It serves the purpose of finding the pointing offsets of the LRI's optical axis with respect to the SC coordinate systems as well as the laser frequency offset, and

Optics EXPRESS

is especially challenging due to the narrow beam width (135 µrad) and limited photodetectors bandwidth (4 to 16 MHz). The initial LOS scan is a search in five degrees of freedom with a parameter space of ±3 mrad for the yaw and pitch angles on each SC —see Fig. 1 for the angles definitions, and 360 MHz for one of the lasers. It will take about 9 hours and will be repeated multiple times at the beginning of the mission to reduce the uncertainty in the parameters estimation. Furthermore, it will be repeated with different instrument configurations to probe the instrument redundancy and *symmetry*. Due to the criticality of this procedure, it has been thoroughly analyzed by simulations [3] and in laboratory experiments in 2014 [4, 5]. However, due to the complexity of the LRI and the SC separation of a few hundred kilometers not all critical parameters involved in the experimental verification were accurately represented. In preceding test campaigns the received (RX) beams, i.e., the ones reaching the far SC after travelling ~220 km, were implemented as Gaussian instead of flat-top beams, which are the expected ones at the SC apertures. Yet, the correct beam profile of the interfering beams plays a significant role on the resulting heterodyne signal and its behaviour under tilts. Furthermore, the received power roll-off as a function of the transmitted beam misalignment was not matched to the expected one and Doppler frequency shifts were not present. In this paper we report our efforts to further validate the LRI LOS calibration procedure by performing tests as realistic as possible and with similar data streams to the ones in the LRI. For this purpose, two mock-up optical benches (OBs) with all the important parameters matching the ones from the flight hardware as well as LRI-type phasemeters (PM) served as models of the SC. In addition, a dedicated set-up, the so called laser link simulator (LLS), which recreates the interspacecraft distance and its effects on the laser beams was developed [6]. The combination of both systems: the mock-up LRIs and the LLS, allowed us to overcome the limitations of the previous experiments. The former (design and construction of the mock-up LRIs) is part of the project *Nanometer Ranging Systems for Low-Earth Orbiter Links* which is located in the collaborative research center 1128 *Relativistic Geodesy and Gravimetry with Quantum Sensors (geo-Q)* while the latter (the LLS) was developed as part of the *Optical Ground Support Equipment* designed for on-ground testing of the LRI.

The manuscript is organized as follows: Section 2 gives an overview of the LRI and the initial acquisition procedure. Section 3 focuses on the experimental set-up description, i.e., the mock-up LRI and the laser link simulator. The tests carried out to validate the LOS calibration procedure together with the results are described in Section 4. A summary of the experiment outcomes is given in Section 5.

Table 1. Nominal parameters for the LRI and GRACE Follow-On

.

Description	Value
SC separation (ℓ)	170 - 270 km
LO Gaussian beam waist (w_0)	2.5 mm
LO beam divergence angle (θ)	135 µrad
Beam radius ($1/e^2$) at far SC (w_{RX})	23 m-36 m
Total local beam power (P_0)	20 mW
Max. RX power per QPR segment (×8)	55 - 136 pW
Doppler shifts (f_D)	±3 MHz
LRI measurement band	2 - 100 mHz

Optics EXPRESS

2. The LRI and the LOS calibration procedure

The LRI —see Fig. 1, realizes a heterodyne laser interferometer link between the two identical GRACE Follow-On SC. Each SC carries an OB and associated electronics, a 1064 nm non-planar ring oscillator (NPRO) laser [7, 8] with an external cavity [9], a triple mirror assembly (TMA) [10, 11] and a laser ranging processor (LRP) that includes a phasemeter (PM) amongst other functionalities [8]. The LRI architecture is based on an offset phase-locked transponder [2]: the laser on the slave SC is offset phase-locked to the frequency stabilized laser on the master SC by means of a digital phase-lock loop implemented in the LRP. This guarantees that the phase of the incoming beam is preserved and at the same time allows to send enough light back to the master SC to realize the interferometric measurement. In this sense the slave SC can be understood as an *amplifying mirror*. The offset phase-locking, at 10 MHz, is needed in order to keep the heterodyne frequencies within the photodetectors bandwidth under the Doppler shifts introduced by the SC relative velocities, which amount to about ±3 MHz. Table 1 summarizes the most important LRI parameters.

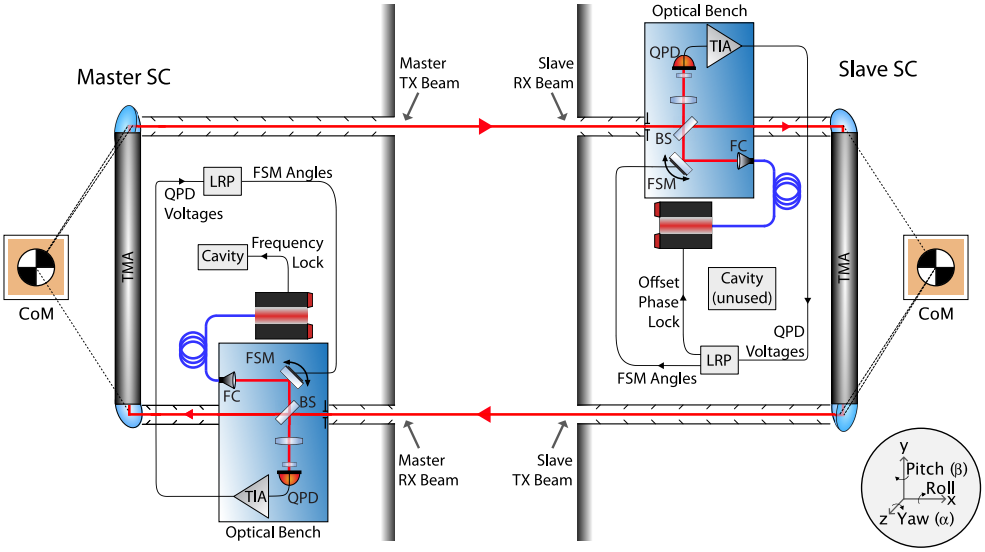

Fig. 1. Schematic drawing of the LRI. Each SC contains one optical bench (OB) together with associated electronics (not shown here), a laser ranging processor (LRP), a laser with external cavity and a triple mirror assembly (TMA) that acts as retroreflector. In nominal operation, the master laser is frequency stabilized to its external cavity whereas the slave laser is offset phase-locked to the received light coming from the master. CoM: center of mass, FSM: fast steering mirror, BS: beam-splitter. FC: fiber collimator, TIA: trans-impedance amplifier, QPD: quadrant photodiode, TX: transmitted, RX: received. At the bottom right corner the used coordinate system is shown. Rotations around the x-axis are called *roll*, rotations around the y-axis are referred to as *pitch* (β) and rotations around the z-axis are called *yaw* (α).

Because the line of the SC centers of mass is blocked by other instruments an off-axis interferometer had to be implemented. In order to keep the tilt-to-length sensitivity low the so-called *racetrack* layout was adopted. The critical unit needed for such a configuration is the TMA, a 60 cm long carbon fibre reinforced plastic (CFRP) tube with three mirrors at the ends, which form a virtual corner-cube retroreflector. The TMA plays a crucial role since it (i) keeps the incoming and outgoing beams aligned, (ii) routes the beam around the cold gas tanks and microwave ranging instrument and, (iii) minimizes the tilt-to-length coupling by

Optics EXPRESS

placing its virtual vertex at the SC center of mass (CoM). Regardless the properties of the TMA, the SC attitude jitter needs to be compensated to maintain the incoming and the local beams aligned. A fast steering mirror (FSM) on each OB is used for this purpose. The angles between the wavefronts of the local oscillator (LO) and the RX beams are constantly measured using differential wavefront sensing (DWS) [12, 13] on both OBs. A control loop implemented on the LRP uses the FSMs to drive these angles to zero. This is crucial since during science operations, both transmitted (TX) beams must at all times point exactly in the direction of the other SC. The unique architecture of the LRI ensures that the two beams are then also aligned to each other locally on the OBs, thus yielding an optimum heterodyne efficiency. Obviously, in order to reach this situation, the laser link must be established first.

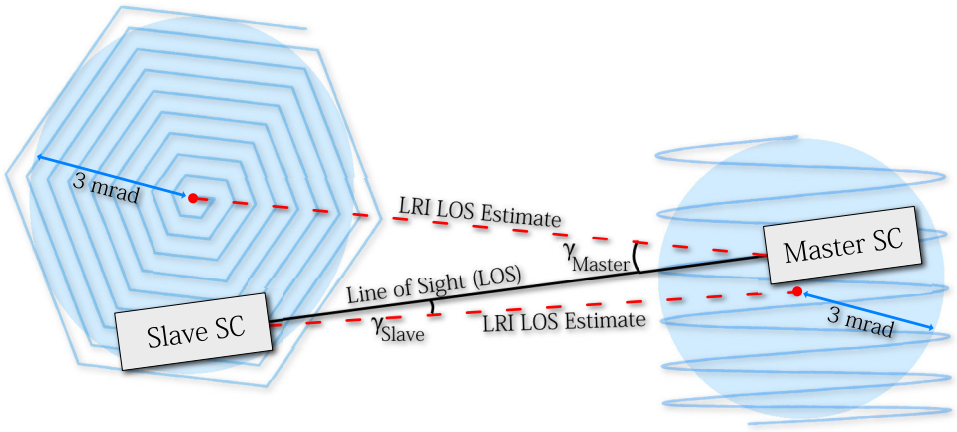

Fig. 2. Schematic drawing of the initial acquisition procedure. Depicted here is the spatial part of the process which serves the purpose of finding the angular offsets between the LRI and the SC. While the SC positions and attitudes are well-known due to star tracker data and orbit predictions, the precise relative orientation of the LRI with respect to these are only known with a limited accuracy. The FSM on the master SC performs a hexagonal scan and at the same time the slave SC scans the TX beam in a Lissajous pattern. Both LRI units are misaligned to the line of sight (LOS) by their corresponding LOS misalignment $\gamma_{\text{Master/Slave}}$, which includes both the yaw and pitch angles.

Alignment tolerances during the LRI integration and SC mechanical shifts caused by the rocket launch result in angle offsets between the SC and LRI coordinate frames —see Fig. 2. The SC attitude information, provided by the star trackers, which is expressed in the SC coordinate frame does thus not deliver helpful information on the LRI coordinate frame. As a result the transmitted laser beams will not be aligned to each other at the beginning of the mission. In addition to the pointing offsets, the two laser frequencies may differ by more than the QPRs' bandwidth. This is a consequence of the different thermal environments of the lasers on board of the two SC, which introduce an uncertainty in their frequencies. None of these effects can be characterized during on-ground testing to the required accuracy and thus, additional calibration of the instrument in orbit is mandatory.

This calibration process is usually referred to as *LOS calibration procedure* or sometimes also as *initial acquisition*. No dedicated hardware is used for this, such as acquisition sensors in the form of CCD sensors [14], amplitude modulation of the RX beams [15] or active re-shaping of the beam profile of the RX beams to ease their detection (so-called *beacon beams* [16]). Instead the procedure simply makes use of the QPRs together with the LRPs as sensors and the FSMs and the lasers as actuators. This is along the lines of the LRI philosophy as a technology demonstrator

Optics EXPRESS

instrument on-board GRACE Follow-On, where many constraints in terms of power, mass, size, etc. were present. In addition, the procedure was designed to be fully compatible with the microwave ranging instrument and not affect its performance.

The angular offsets are found by performing synchronized two-dimensional spatial scans with both FSMs and a laser frequency scan on the slave SC while the master laser is locked to its optical cavity —see Fig. 2. During this process both LRPs continuously compute fast Fourier transforms (FFTs) of the signals on the QPRs, which are simply noise unless the five degrees of freedom (four angles and laser frequencies) are within a narrow range simultaneously: ~135 µrad for the angles and 4 to 16 MHz for the heterodyne frequencies [2]. The hierarchy of the scans is the following: the frequency scan is carried out as a linear ramp of the slave laser where each frequency is only covered once, the master SC scans its yaw, α, and pitch, β, angles using the FSM in a discrete hexagonal pattern. For each of the hexagonal steps the slave SC does a complete fast Lissajous scan. The ramp of the frequency scan is chosen such that the heterodyne frequency is not pushed out of the QPR bandwidth within one hexagonal scan. The Lissajous scan pattern is realized by performing synchronous sinusoidal motions in both FSM axes. Table 2 lists all the parameters of the scans and Fig. 3 shows the scans and the grid errors for the Lissajous and hexagonal patterns. The grid error is defined as the maximum distance from any point to the nearest scan point.

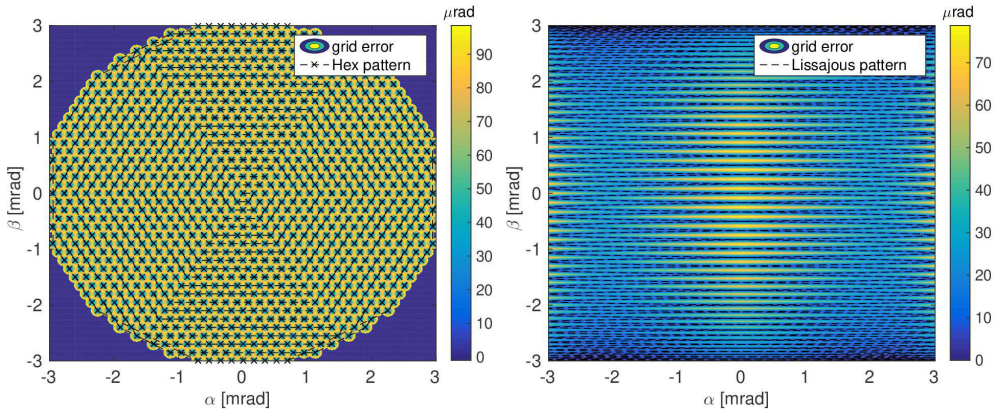

Fig. 3. LRI scan patterns (dashed black lines) and their grid errors (color coded). Left: The local FSM on the master SC does a hexagonal pattern. Right: Lissajous scan pattern of the slave SC FSM.

Initial acquisition is a scheduled process that requires commanding from ground. At the programmed time, the LRI performs the previously detailed sequences simultaneously and synchronized on both SC. After having scanned the complete parameter space the FFT results, the corresponding FSM positions as well as the laser thermal set-points and the time stamps are sent to ground, where the data are processed together with SC attitude and temperature information in order to estimate the LRI angular offsets and laser thermal set-point. The data will contain all detected FFT amplitude peaks above a preset threshold. This process can be repeated a few times to reduce uncertainties. Once reliable values for the coordinate system and frequency offsets have been identified, these parameters will be uploaded to the SC.

This procedure ensures that all static offsets have been accounted for. However, all five previously determined parameters also have a time-dependent component and contain uncertainties due to, e.g., grid error, star trackers or orbit prediction. Therefore, a subsequent *re-acquisition scan* is still required before the laser link can be established. This is a 80-second autonomous scan similar to the initial scan but with a reduced parameter space (±300 µrad and 320 MHz) and with the pointing and frequency set-point information from the LOS calibration scans as a starting

Optics EXPRESS

Table 2. LRI nominal parameters for the LOS calibration procedure

.

	Master	**Slave**	
Parameter	Spatial Scan	Frequency Scan	Spatial Scan
Scan type	Hexagonal	Linear ramp	Lissajous
Scan range	±3 mrad	360 MHz	±3 mrad
Grid error	100 µrad	n.a.	84 µrad (max.)
Scan time	627 s	9 hrs	0.56 s
Rate	1.6 mHz	11 kHz/s	f_α = 100 Hz f_β = 1.79 Hz

point. The parameter space of the angular scan is reduced drastically because the large scan amplitudes covered by the LOS calibration are mainly due to static effects. Thus, it is not required to re-scan such large uncertainties during re-acquisition. The laser frequency, however, is highly dependent on temperature. Thus, the offset of the slave and master laser frequencies can be almost as large as the one during the initial LOS scans. Therefore, the frequency scan range is only reduced marginally. However, a large peak in the FFT spectrum causes the SC to immediately abort the re-acquisition scan and to transition into a state where the five degrees of freedom are within the operating working limits. At this point both SC switch to the so called *science mode*, where the digital phase-lock loop keeps the slave laser offset phase-locked to the master laser and the FSMs keep the beams co-aligned by zeroing the DWS signals regardless the SC attitude jitter. From this point on read-out of the optical phases is possible and thus, information on the intersatellite range is available. Each time the lock is lost the LRI automatically transitions to the re-acquisition state which, should re-enable the science state within a short period of time.

3. Experimental setup

This section describes the two main parts of the set-up: the mock-up LRI and the LLS. A detailed diagram of the set-up is shown in Fig. 4. The LLS recreates the optical link between the SC while the mock-up LRI simulates the actual LRI. The whole set-up was standing on two optical tables (pneumatic vibration isolation) in a temperature controlled (±0.5°C) laboratory.

3.1. The laser link simulator

The LLS serves the purpose of recreating the laser link between the two satellites (or subsets of the LRI) for on-ground testing purposes and LOS calibration experiments. In order to fulfill this task, the LLS has the following functionalities: simulate the power drop in the RX beam as a function of the misalignment between the LRIs optical axis, introduce SC attitude jitter, introduce static LOS misalignments, generate Doppler shifts and generate flat-top beams at the receiving apertures. The functionalities have been implemented in the following manner: the angle of the TX beam leaving one mock-up LRI is measured by means of the LLS quadrant photo-detector (QPD) using a small fraction of the light being transmitted to the far SC. The angles measured by the QPD correspond to the ones introduced by the FSM with respect to the LOS. The rest of the light is launched into an optical fiber with the help of a fiber collimator specifically chosen to have a large acceptance angle. Doppler shifts, which occur due to the relative velocity between the SC, are imprinted onto the laser light by means of two acousto-optical modulators (AOMs) with nominal operating frequencies of −75/+85 MHz. The power level sent to the far SC is attenuated as a function of the TX beam angle to match the predicted value for a given SC separation. The attenuation is performed by a static fiber optical attenuator in conjunction with a

Optics EXPRESS

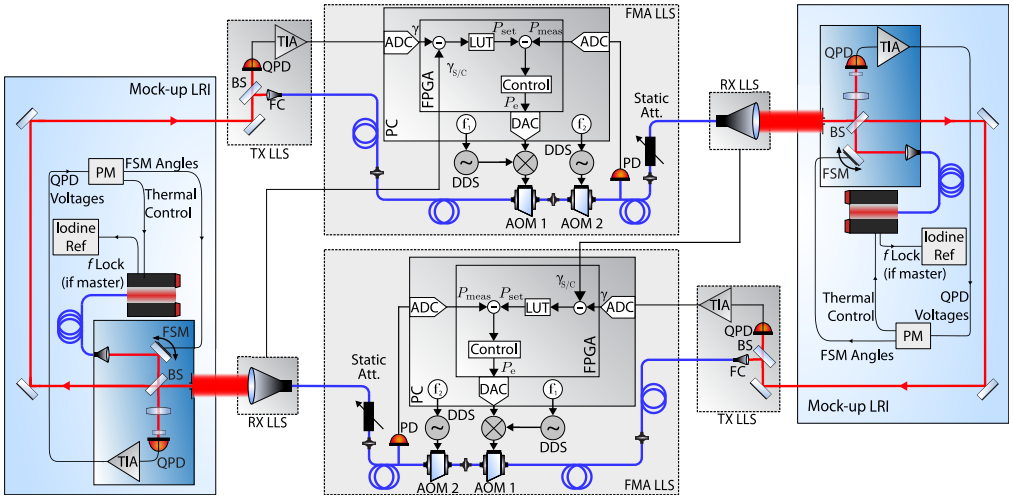

Fig. 4. Experimental set-up: two mock-up LRIs, each containing one OB, PM and a laser. The master laser is frequency stabilized to an iodine reference whereas the slave laser is free running. The LLS simulates the 220 km link between the SC. It can be split into a TX and RX part as well as a frequency modulation and power attenuation (FMA) part. See [6] for details. ADC: analog-to-digital converter. BS: beam-splitter. FC: fiber collimator. DDS: direct digital synthesizer. FPGA: field programmable gate array. LUT: look-up table. DAC: digital-to-analog converter. AOM: acousto-optical modulator.

closed loop system that measures the power delivered to the far SC and corrects it by modulating the rf power driving the AOMs. The control loop has a bandwidth of ~50 kHz and reproduces accurately the power drop in the RX beam even when the fast Lissajous scan is present. The RX beam is imitated by using a large fiber collimator, which creates a Gaussian beam with a waist of $w_0 \simeq 16$ mm, and thus exhibits a sufficiently homogeneous intensity profile and flat wavefront over the 8 mm SC receiving aperture —see Fig. 5 (left panel), since the total power in the aperture is ~6% smaller and the heterodyne efficiency is ~5% higher compared to the ideal flat-top beam case. LOS misalignments are introduced by means of motorized stages on the RX and TX ports. The recreation of the RX power drop as a function of the LOS angle is shown in Fig. 5 (right): the top figure shows the Lissajous scan and the power distribution in the spatial domain while the bottom plot shows the equivalent figure in the time domain. The power drop model is

$$P_{\mathrm{RX}} = 2P\frac{r_{\mathrm{ap}}^2}{w_{\mathrm{RX}}^2}e^{-2[(\alpha-\alpha_0)^2+(\beta-\beta_0)^2]\ell^2/w_{\mathrm{RX}}^2} \tag{1}$$

where $P \simeq 18$ mW is the power leaving the SC, $r_{\mathrm{ap}} = 4$ mm is the radius of the OB aperture, α_0 and β_0 are the LOS misalignment angles in yaw and pitch, respectively, α and β are the FSM angles with respect to the LOS, $w_{\mathrm{RX}} \simeq 30$ m is the waist of the beam when reaching the far SC and $\ell \simeq 220$ km is the interspacecraft distance.

3.2. Mock-up LRI

The only parts of the LRI —see Fig. 1, needed for this test campaign were two lasers, two phasemeters and two OBs. The TMAs were substituted by two mirrors since, in principle, they do not play a role in the LOS calibration procedure. The RX beam generated by the LLS is clipped by an 8 mm aperture on each OB. It is then interfered with the local beam on the recombination beam-splitter. A two lens imaging system is used to image the FSM pivot point and the aperture on the QPD, effectively suppressing beamwalk of the RX and LO beams on the InGaAs quadrant

Optics EXPRESS

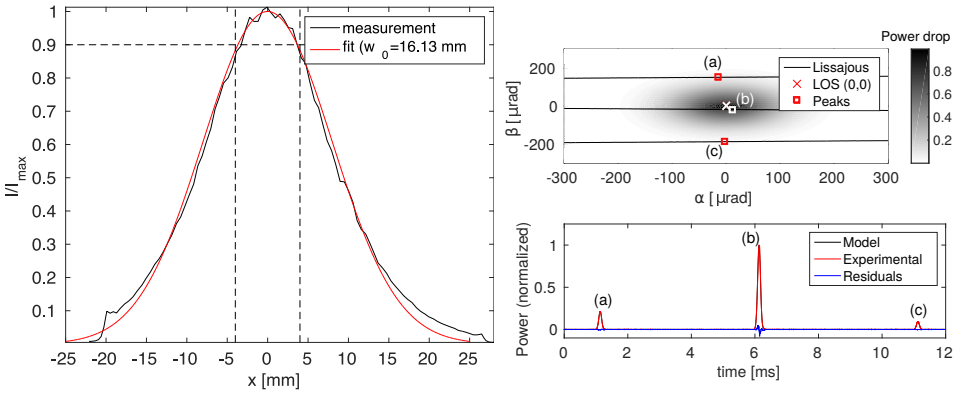

Fig. 5. Left: RX flat-top beam generated by the LLS. The intensity profile within the OB aperture (r_{ap} = 4 mm) drops only by 10%. Right top: zoom of the Lissajous scan and power distribution around the LOS (in this example located at $\alpha_0 = \beta_0 = 0$ µrad and shown as a cross) —see Eq. (1). Right bottom: shows the theoretical and the reproduced by the LLS received power as a function of time when a Lissajous scan is present. The amplitude of the highest peak when coinciding exactly with the LOS is between 440 pW and 1000 pW, depending on the SC separation.

photodiode. The re-combination beam-splitter reflects 90% of the LO beam towards the mirrors, which then deflect the beam in the direction of the TX LLS unit. Wherever possible, the same parameters as for the flight models of the OBs were used (namely the splitting ratio of the beam-splitter, lens parameters and QPR layout and components). The main difference with respect to the LRI OB is the absence of a redundant QPR.

For each OB the read-out of the optical phases, the control of the two mechanical axes of the FSM on the OBs as well as the control of the slave laser frequency (where this was required) was done with the help of PMs developed for this purpose, which have the same architecture as the ones on-board GRACE Follow-On [17]. For the LOS calibration tests the PMs did not measure the phase of the incoming signal since the link had not yet been established. Instead FFTs with a length of 4096 points at a sampling rate of 40 MHz were continuously computed as it will be done by the LRP on-board the LRI [8]. The FFT length was optimized with respect to the expected duration of a detected flash during initial acquisition, which is a result of the fast component of the Lissajous scan —see Fig. 5 (right panel) where the fast flashes, ~200 µs in duration, are shown. The amplitudes and frequencies of the FFTs were sent to a computer where they were stored at a frequency resolution of 40 MHz/4096≃10 kHz when short measurements were taken. For complete LOS calibration tests the data size was reduced by storing only the points corresponding to the 100 largest FFT amplitudes.

3.3. *Fine steering mirror characterization*

As previously stated the goal of the LOS calibration is to estimate the misalignment between the optical axis of the LRI and the SC reference frame by performing an angular scan with the FSMs. When their position compensate for the local misalignments both beams are aligned. At such position the FFTs in both OBs exhibit a signal above the noise level assuming the lasers frequencies are between 4 and 16 MHz. The FSMs' positions, after taking into account the SC attitude information, correspond to the LOS misalignment. Consequently, one needs to know accurately the FSM position when the FFT peaks occur. In the LRI this is accomplished by actually measuring the position of the mirror using a high-speed sensor. In our set-up, we only had access to the commanding signals, which is not a problem when the driving signals are

Optics EXPRESS

well below 100 Hz. Otherwise, gain peaking and phase delay causes the commanding and actual position to differ significantly. This issue was mitigated by measuring the FSM transfer function —see Fig. 6 (left panel), and correcting its effects in post-processing by applying the gain and phase to the ideal commanding signal, i.e.,

$$\alpha_{\text{corr}} = A \cdot G \cdot \sin(2\pi f_\alpha t + \phi), \tag{2}$$

where A is the commanded amplitude and $f_\alpha = 100$ Hz the frequency of the fast axis, yaw (α), in the Lissajous scan. G and ϕ are the gain and phase at $f_\alpha = 100$ Hz obtained from the transfer function. They are $G = 1.14$ and $\phi = 0.23$ rad. Figure 6 (right panel) shows the errors without applying the correction: they are within ±800 µrad, which are above the maximum errors allowed for re-acquisition, i.e., ±300 µrad as described in Sec. 2.

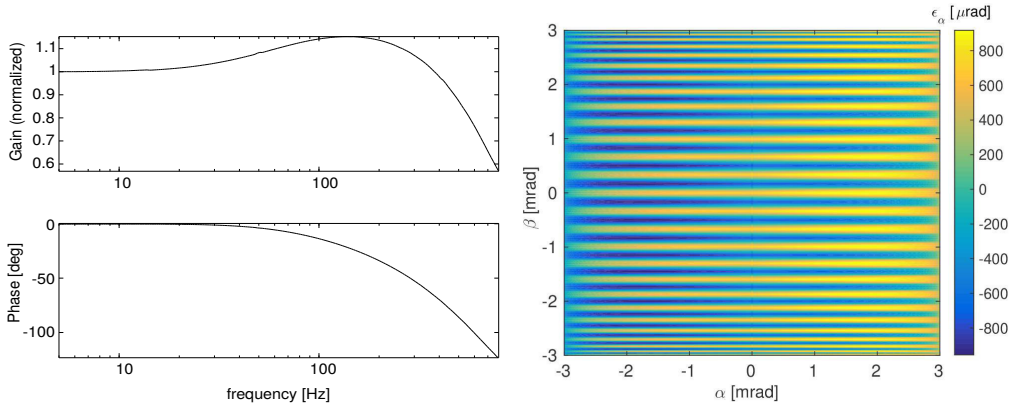

Fig. 6. Left: Transfer function of the FSM used in the mock-up LRI. Right: errors in the fast angle, yaw (α), between commanded and actual angles when a Lissajous scan is performed with $f_\alpha = 100$ Hz, $f_\beta = 100/56 = 1.7857$ Hz and an amplitude of $A = 3$ mrad. The errors due to the mock-up LRI FSM transfer function in the yaw angle can be as high as 800 µrad, which is almost an order of magnitude higher than the grid errors and thus, needs to be corrected in post-processing.

3.4. Carrier-to-noise density

A figure of merit, which is often used to compare (received) signal strengths, is the so-called *carrier-to-noise density* (C/N_0). It has units of dB-Hz and is defined as

$$C/N_0 = 10\log_{10}\left(\frac{A_c^2/2}{S_n}\right), \tag{3}$$

where A_c is the peak amplitude of the *carrier* signal and S_n is the power spectral density (PSD) of the measurement noise at the frequency of the carrier. In our case, the term A_c corresponds to the signal generated at the QPRs when the local beam and the receiving beam interfere, or:

$$A_c = 2\mathcal{R}\sqrt{P_{LO}P_{RX}\eta}, \tag{4}$$

where $\mathcal{R}$ is the InGaAs photoreceiver responsivity, i.e., 0.7 A W^{-1} (at 1064 nm) [18]. P_{LO} is the fraction of the local beam power used to interfere with the receiving beam and corresponds only to 10% of P_0, i.e., 2 mW for the nominal case. The rest of the light, 18 mW, is sent to the far SC as described in Sec. 2. P_{RX} is the receiving power from the far SC and depends on the misalignment between the transmitting beam and the SC line-of-sight, and their separation

Optics EXPRESS

—see Eq. (1). The maximum received power in the LRI, i.e, for a perfect alignment between the transmitted beams and the LOS spans between 440 pW and 1000 pW for SC separation of 170 km and 270 km, respectively. The term η corresponds to the heterodyne efficiency, a value between 0 and 1, which describes the spatial overlap and the mode match of the local and RX laser beams and strongly depends on their wavefront alignment and mode content. For a perfect alignment, A_c is in the order of 1.5 μA_{pk}.

S_n is composed of three terms: photoreceiver current noise, laser shot noise and laser noise due to relative intensity noise (RIN). They all can be considered white noise in the QPRs and PM range, 4 MHz to 16 MHz. Their PSDs are added together as:

$$S_n = 4S_i + 2q\mathcal{R}P_{LO} + (\mathcal{R}\,P_{LO}RIN)^2, \tag{5}$$

where $S_i = (9.8 \times 10^{-12})^2$ A^2 Hz^{-1} is the photodetector dark current per quadrant and the factor of 4 accounts for the four segments of the QPR, $q = 1.6 \times 10^{-19}$ C is the elementary charge and $RIN = 3 \times 10^{-8}$ Hz$^{-1/2}$ is the relative intensity noise of the NPRO laser. The shot-noise and RIN introduced by the RX beam are neglected since they are orders of magnitude below the ones introduced by the local beam. Substituting terms in Eq. (5) yields $S_n = 2.6 \times 10^{-21}$ A^2 Hz^{-1}, which is very similar to the LRI one: $S_n = 2.4 \times 10^{-21}$ A^2 Hz^{-1} [18].

The expected minimum C/N_0 value that allows to detect a signal is about 60 dB-Hz, which is derived from worst-case conditions considering grid errors, FFT scalloping losses, non-constant amplitudes while scanning, laser power variations, SC separation, etc. Since our experimental set-up should be a very accurate model of the LRI, the LOS calibration signals should deliver C/N_0 levels in the $\sim$ 60 dB-Hz range, comparably to the expected signals during the LRI commissioning phase, and thus it provides quantitative indication of the faithfulness of the experimental set-up and LOS calibration procedure recreation.

4. Line of sight calibration tests

The LOS calibration tests consisted of: (i) applying different misalignments between the SC LOS and the LRI optical axis, (ii) recreating the LOS calibration scans and, (iii) analyzing the data in post-processing to estimate the misalignments from the data in a similar way it will be done in flight. First, tests were carried out with only one laser whose light was distributed to both OBs. Thus, rendering the frequency scan redundant and, consequently, reducing significantly the time required for each scan —see Sec. 4.1. Complete tests with two independent laser sources including spatial and frequency scans are described in Sec. 4.2.

4.1. Tests with one laser

The set-up for the tests with one laser is shown in Fig. 7. The offsets between the optical axes of the OBs and the SC LOS were realized by misaligning the LLS with respect to the OBs in the following manner: the RX beam was rotated by the motorized stages by an amount known better than ~50 µrad. At the same time the TX beam assembly holding the QPD was aligned to RX beam by rotating it by the same amount, i.e., by centering the beam in the QPD and maximizing the light coupled into the fiber collimator. The goal of the test was, first, to detect the flashes and, second, to infer the introduced misalignment angles. Note that now both master and slave OB only detect a signal when each FSM has compensated its own OB misalignment with respect to the LOS. The frequency shifts needed between the OBs to generate the heterodyne signals within the QPRs bandwidth were introduced by the AOMs and kept fixed at 10 MHz.

Multiple scan amplitudes and corresponding grid errors were tested with low power levels: 80 pW per quadrant, i.e., a total of 320 pW. In the LRI nominal conditions the lowest received power will be in the order of 440 pW (for ℓ = 270 km). The local oscillator power, P_{LO}, was 18 mW, exactly as in the LRI. Figure 8 shows an example of detections made during these

Optics EXPRESS

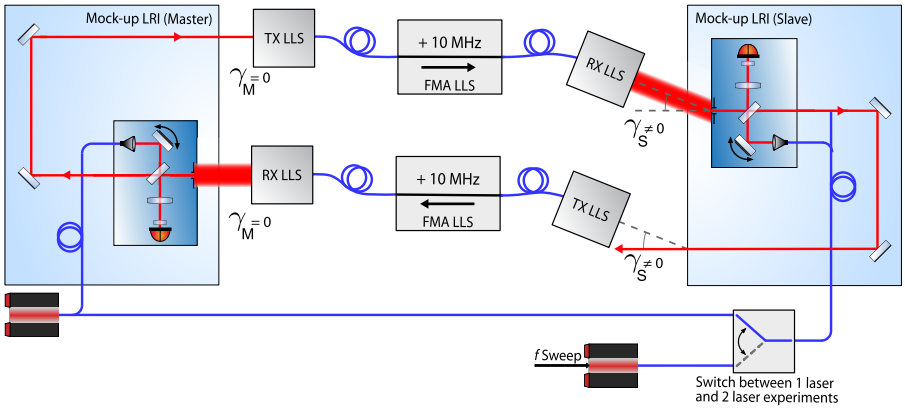

Fig. 7. Experimental set-up for the LOS calibration procedure. γ represents the introduced (and known) LOS misalignment of one of the mock-up LRIs in either yaw, α_0, or pitch, β_0. During test runs with only one laser, a flash during the scan is detected if the spatial misalignment of the mock-up LRIs are corrected by the FSMs by amounts equal to γ_S and γ_M. When both lasers are used, also the frequency of the slave laser needs to match the master laser frequency for a flash to occur. Note that the figure shows both configurations: with one and with two lasers. The switch shown at the bottom right is not physically included in the experiment. It is simply drawn here to illustrate the possiblity of supplying the slave mock-up LRI with the laser from the master LRI *or* with its own laser source.

experiments. It can be seen that the detections (flashes) with maximum amplitudes happened at a frequency of 10 MHz and $C/N_0 \simeq 70$ dB-Hz, which is consistent with the expected values.

Figure 9 gives an overview of the results and shows for each run: (i) the introduced LOS misalignments (in light purple and light blue), (ii) the estimated misalignments (in dark purple and dark blue) after correcting the yaw angle of the Lissajous scan as described in Sec. 3.3 and (iii) the C/N_0 levels. Scans were declared successful when both OBs showed clear detections and when the half-cone angle of the LOS was estimated with an error less than 300 µrad, i.e.,

$$[(\hat{\alpha}_0 - \alpha_0)^2 + (\hat{\beta}_0 - \beta_0)^2]^{1/2} \leq 300\,\mu\text{rad} \tag{6}$$

where $\hat{\alpha}_0$, $\hat{\beta}_0$ represent the estimated LOS misalignments from the FSM commanding signal and α_0, β_0 the introduced LOS misalignemnts. The 300 µrad threshold corresponds to the range of the re-acquisition scan, which is carried out after the LOS calibration procedure and that eventually leads to the science mode autonomously —see Sec. 2. Two unsuccessful runs occurred at the master OB (hexagonal scan) due to no flash detection (indicated with a C/N_0 value of "–.–" in red). On the slave OB scan (Lissajous scan) three errors occurred, two of them due to no flash detection and one for having an error slightly larger than 300 µrad: 360 µrad (shown in red). All unsuccessful runs happened when the grid errors of the scan patterns were set to 140 µrad, instead of the nominal LRI ones of 100 µrad and 84 µrad for the hexagonal and Lissajous scans, respectively. The fact of using a rather large grid error and low received power led to signals closer to the C/N_0 limit and thus, in some cases, they became indistinguishable from the noise. For the successful runs, the half-cone errors were between 20 µrad and 160 µrad for the hexagonal scan and between 10 µrad and 290 µrad for the Lissajous one. These errors are a combination of grid error, uncertainty in the introduced LOS misalignments and FSM transfer function correction. Overall most of the runs were successful and delivered acceptable estimates of the LOS misalignments.

Optics EXPRESS

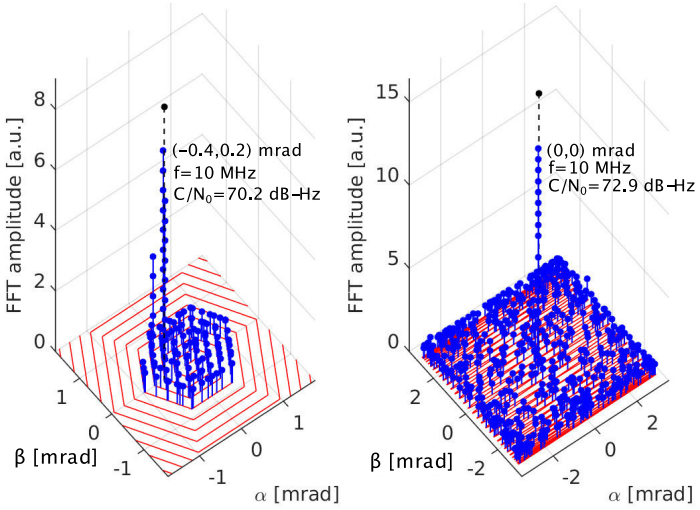

Fig. 8. Example of a detection during one of the measurement runs. The FFT amplitudes of the master (left) and slave (right) scans are plotted as a function of the FSM angles. Both flashes occurred at a heterodyne frequency of 10 MHz and $C/N_0 s$ of the order of 70 dB-Hz. The true LOS values are represented by the black-dashed trace: $\alpha_{0,\mathrm{M}} = -0.5$ mrad, $\beta_{0,\mathrm{M}} = 0$ mrad, $\alpha_{0,\mathrm{S}} = 0$ mrad and $\beta_{0,\mathrm{S}} = 0$ mrad. The estimated values are: $\hat{\alpha}_{0,\mathrm{M}} = -0.4$ mrad, $\hat{\beta}_{0,\mathrm{M}} = +0.2$ mrad, $\hat{\alpha}_{0,\mathrm{S}} = \hat{\beta}_{0,\mathrm{S}}$=0 mrad.

4.2. *Tests with two independent lasers*

The LOS calibration procedure tests including two independent laser sources with frequency and spatial scans were carried out using the configuration shown also in Fig. 7. This set-up allows for a full LOS test, i.e., with spatial and frequency scans. In this situation a flash during the scan is detected if the misalignments of the mock-up LRIs are corrected by the FSMs by an amount equal to γ_{S} and γ_{M} and the heterodyne frequencies are within the QPRs bandwidth. The laser on the master OB was therefore stabilized to an iodine hyperfine line reference that mimicked the optical cavity in the LRI master SC. The laser on the slave OB consisted of a free-running laser. The Doppler frequency was kept fix at $f_{\mathrm{D}} = 10$ MHz, which is significantly higher than the LRI one, ±3 MHz. The reason was because the frequencies of the two AOMs in series (see Fig. 4) to generate the Doppler shifts were separated by 10 MHz (−75/+85 MHz). Nevertheless, this should not affect the validity of the experiments presented here.

The first tests consisted of an angular scan while the two lasers frequencies where kept within the QPRs bandwidth, i.e., no actual frequency scan was present. These tests were equivalent to the ones described in Sec. 4.1 but using two independent lasers, of which one was drifting and thus affecting the heterodyne frequencies. The received power was again 80 pW per quadrant. The amplitude of the hexagonal and Lissajous scans was set to 1.5 mrad, causing the grid errors to change to 100 µrad to match the LRI one (hexagonal scan), and 50 µrad, which is slightly smaller than the actual LRI one of 84 µrad for the Lissajous scan. The LOS misalignments for all the following runs were set to

Two independent representative measurements are shown in Fig. 10(i) and 10(ii). For these tests only the points corresponding to the ones having the 100 highest FFT amplitudes were stored. Still, most of them were simply noise and were also discarded in post-processing. The

Optics EXPRESS

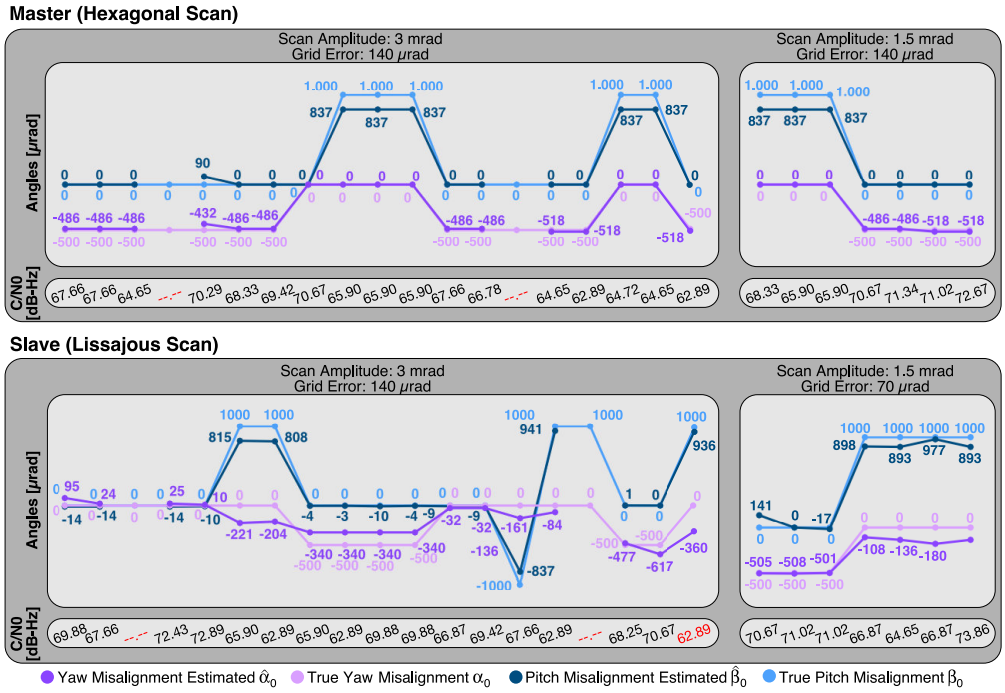

Fig. 9. Summary of the scans with two optical benches and one laser, i.e, only spatial scan. Top panel: master OB (hexagonal scan). Bottom: slave OB (Lissajous scan). The colored numbers along the course of the curves indicate the angles in μrad. The C/N_0 values for each of the runs are also shown in units of dB-Hz below the respective plots and as expected they increased in both OBs when reducing the grid error of the Lissajous scan.

Table 3. **Introduced LOS misalignments**.

Master		Slave	
$\alpha_{0,\mathrm{M}}$	$\beta_{0,\mathrm{M}}$	$\alpha_{0,\mathrm{S}}$	$\beta_{0,\mathrm{S}}$
0 μrad	+1000 μrad	−500 μrad	0 μrad

ones shown in Fig. 10 were kept since their amplitudes were above the noise levels and their frequencies within the QPR and phasemeter bandwidth. Flashes were clearly visible in both runs with C/N_0 values around 69 dB-Hz. The FSMs positions at the peaks agreed well with the introduced LOS misalignments. An unexpected detection with a small FFT amplitude occurred at the slave FSM position of $\hat{\alpha}_{0,\mathrm{S}} = -860\,\mu$rad and $\hat{\beta}_{0,\mathrm{S}} = 0\,\mu$rad. The presence of a flash at such position is not completely understood, but it is probably related to the FSM driving and post-processing correction —see Sec. 3.3. Anyhow, by considering only the highest peaks the LOS misalignments were properly estimated for the four angles.

Finally, an actual frequency scan was introduced to put to test the complete LOS calibration procedure. All the parameters were kept the same but here the lasers frequencies were initially separated by about 35 MHz. This allowed us to perform the tests in a reduced amount of time (about one hour) without compromising the outcomes of the experiments. The slave laser frequency was scanned at an average rate of 12.5 kHz s^{-1}. The results for two trials are shown in Fig. 11. The top one 11(iii) was performed with low power levels (80 pW per quadrant), while in

Optics EXPRESS

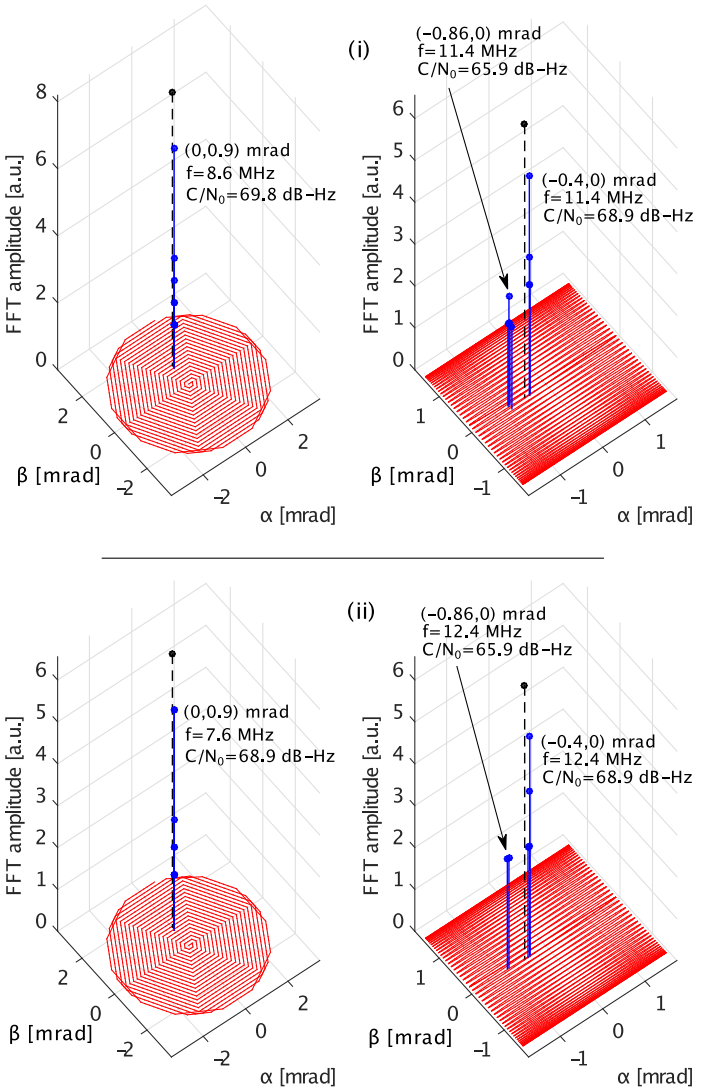

Fig. 10. Two examples of spatial scanning detections when using two independent lasers but without frequency scan. The lasers were set to be within the QPRs bandwidth at the starting of the spatial scan. The master laser was locked to a iodine frequency standard, while the slave one was left free running. The true LOS values are represented by the black-dashed trace: $\alpha_{0,\mathrm{M}} = 0$ mrad, $\beta_{0,\mathrm{M}} = 1$ mrad, $\alpha_{0,\mathrm{S}} = -0.5$ mrad and $\beta_{0,\mathrm{S}} = 0$ mrad. The estimated values for the master and slave mock-up LRIs are given in parenthesis ($\hat{\alpha}$, $\hat{\beta}$).

the bottom one 11(iv) the power was increased to 135 pW per quadrant, i.e., 540 pW in total, which is equivalent to a SC separation of $\ell = 240$ km. The estimated LOS misalignments from measurement 11(iii) agreed well with the true values, except again in the fast Lissajous angle, α, where two positions with similar FFT amplitudes: -380 µrad and -860 µrad were detected. Such behavior was already detected in the previous measurement and it is assumed to be related to the set-up and, specifically to the FSM driving and post-processing correction. The results obtained when increasing the received power —see Fig. 11(iv), show, as expected, a C/N_0 increase by about 2-3 dB-Hz and, thus clearer detections. In addition, the uncertainty in the fast angle of

Optics EXPRESS

the Lissajous scan was also reduced: the highest peak was located at $\hat{\alpha}_{0,\mathrm{S}} = -600\,\mu\mathrm{rad}$ and $\hat{\beta}_{0,\mathrm{S}} = -100\,\mu\mathrm{rad}$. The second largest peak was at $\hat{\alpha}_{0,\mathrm{S}} = -400\,\mu\mathrm{rad}$ and $\hat{\beta}_{0,\mathrm{S}} = 0\,\mu\mathrm{rad}$.

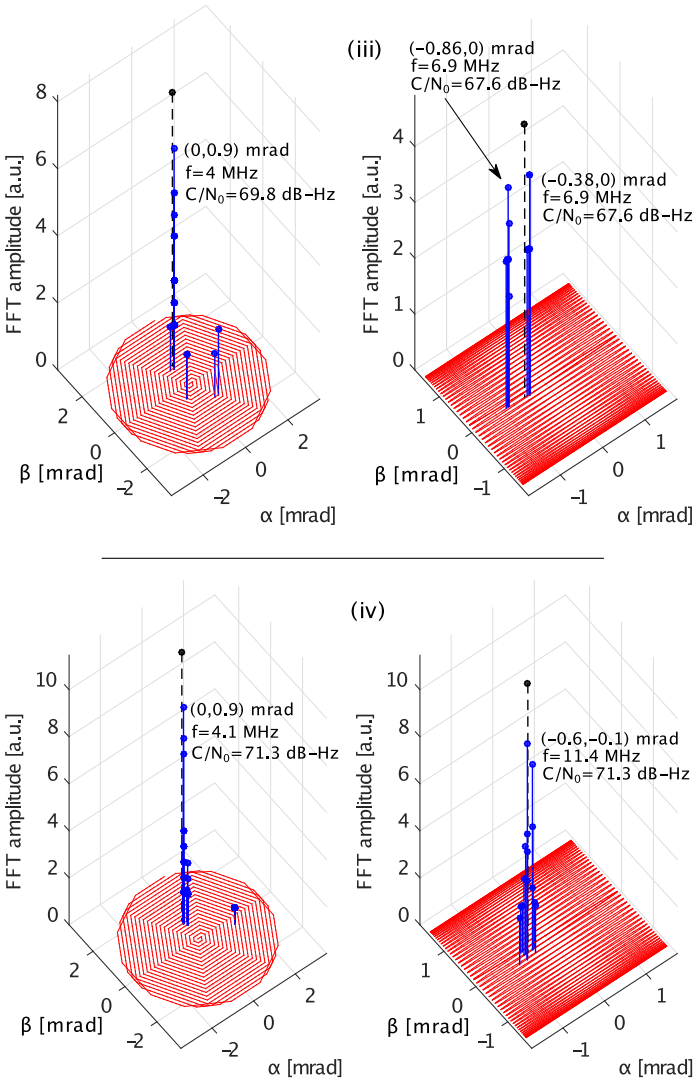

Fig. 11. Two examples of data including frequency and spatial scans. Left: 80 pW per quadrant. Right: 135 pW per quadrant. Lasers were about 35 MHz apart at the beginning of the scan. The master laser was locked to the iodine frequency standard reference, while the slave performed a frequency scan at a rate of 12.5 kHz s^{-1}. The true LOS values are represented by the black-dashed trace: $\alpha_{0,\mathrm{M}} = 0\,\mathrm{mrad}$, $\beta_{0,\mathrm{M}} = 1\,\mathrm{mrad}$, $\alpha_{0,\mathrm{S}} = -0.5\,\mathrm{mrad}$ and $\beta_{0,\mathrm{S}} = 0\,\mathrm{mrad}$. The estimated values for the master and slave mock-up LRIs are given in parenthesis $(\hat{\alpha}, \hat{\beta})$.

5. Summary

We have experimentally validated the LOS calibration procedure to be performed by the LRI on-board the GRACE Follow-On mission in its commissioning phase in the summer of 2018. The results presented here represent a step further in the experimental verification since they

Optics EXPRESS

include conditions not considered in previous experiments, i.e., realistic received power levels by the SC as a function of the misalignments, use of flat-top beams as received beams and Doppler frequency shifts. In addition, the used hardware (optical benches including photoreceivers and fast steering mirrors, phasemeters and lasers) thereby served as proper mock-ups of the LRI and the measurement data was obtained and stored in similar way as it will happen through the real LRI.

Different configurations and spatial scans have been tested. The detections and estimated LOS were in good agreement with expectations, even though the received powers were set to be slightly lower than the expected ones in flight. Only the fast angle of the Lissajous scan has shown some flashes with low amplitude at unexpected FSM positions, which were not completely understood but seem to be related to our set-up and steering mirror limitations and should not be present in the LRI flight version.

Overall, the results obtained in this test campaign validate the robustness of the initial line of sight calibration procedure and provide insights to the whole GRACE Follow-On LRI team in the process of preparing for the in-orbit calibration procedure. This should enable the first ever inter-spacecraft laser interferometer and pave the way for the next generation of gravity field missions and provide valuable data for the future gravitational wave detector in space, the laser interferometer space antenna (LISA).

Finally, the test set-up can serve as part of a ground reference model of the LRI, which can be used as test-bed for debugging and testing if the LRI encounters problems or shows peculiarities in orbit.

Funding

Bundesministerium für Bildung und Forschung (BMBF), project number 03F0654B; Deutsche Forschungsgemeinschaft (DFG), Sonderforschungsbereich (SFB) 1128 Relativistic Geodesy and Gravimetry with Quantum Sensors (geo-Q).